Automated Site Extraction for Scan-to-BIM Progress Monitoring in Road Network Construction

Ziang Jiang[1], Xuesong Shen[1], Khalegh Barati[1] and James Linke[2]

[1]School of Civil and Environmental Engineering, The University of New South Wales (UNSW), Australia
[2]GeoAI, Australia
ziang.jiang@unsw.edu.au, x.shen@unsw.edu.au, khalegh.barati@unsw.edu.au, j.linke@llsurveys.com.au

Abstract –

Construction progress monitoring is an essential activity for ensuring a project's quality and timely delivery. Scan-to-BIM demonstrates its potential and superiority in capturing the as-built status and handling design changes to achieve real-time project tracking. Previous studies have focused on its main steps, including segmentation, recognition, and reconstruction, but often overlooked target area extraction due to their emphasis on residential buildings. Manual extraction can be tedious, time-consuming, and labor-intensive, especially for large-scale, horizontal transport infrastructures. Although similar applications can be found in other domains, these methods may not be feasible for extracting road networks construction sites due to differences in data structure, the as-built status of roads, and the requirements for the Level of Detail (LoD) in the output. This paper proposes an automated hybrid road construction site extraction framework as the input for subsequent Scan-to-BIM construction progress monitoring. It leverages both local feature analysis and graph theory. The developed road patch generation and connection processes enable the extraction of complex road networks with high generality and versatility. Two sets of Airborne Laser Scanning (ALS) data with different construction progress were used to validate the proposed framework, achieving site extraction accuracies of 99.59% and 94.50%, respectively. These results indicate that the proposed method can effectively serve as a basis for supporting construction progress monitoring through Scan-to-BIM.

Keywords –

Point Cloud; Airborne Laser Scanning; Road Construction; Sit Extraction; Construction Progress Monitoring; Scan-to-BIM

1 Introduction

Frequent project monitoring is crucial for improving performance in the construction and renovation of transport infrastructure [1, 2]. It was reported that recent studies have focused on achieving project monitoring by creating as-built models for structures under construction [3-5]. Indeed, numerous road network extraction approaches can be found in the domains of remote sensing and computer vision, serving as the modeling foundation for supporting transport network design, analysis, optimization, and the generation of high-definition (HD) maps for autonomous driving [6, 7].

Ground-based Mobile Laser Scanning (MLS) and aerial images have been commonly used as primary data sources for modeling urban streets and highway systems in previous studies. However, these sensors are insufficient for capturing complex, large-scale transport infrastructure construction sites in terms of efficiency. As an alternative, ALS demonstrates superiority in road classification for complex environments compared to orthoimages [8]. Although learning-based methods have achieved advancements in object recognition, the lack of training datasets and the complexity of site environments—such as ruts, temporary roads, hills, and trenches—affect the performance of common classifiers developed for photogrammetry and laser scanning [9-12]. Additionally, these site conditions hinder the application of conventional image processing methods, such as edge detection or line fitting. Similarly, many widely used local feature analysis methods, including plane fitting and gradient mapping, face the same challenges. Due to differences in primary data sources, the targeted stages of a road's life cycle, and the expected output based on application requirements, a research gap exists. Currently, no proper automatic method for effectively extracting road networks at construction sites has been developed to support Scan-to-BIM construction progress monitoring through ALS.

The proposed hybrid methodology aims to achieve automated road construction site extraction, starting from the earthwork stage. This methodology is characterized by two key academic contributions: (1) automated site extraction for road construction with complex layouts; and (2) high generality and adaptability to complex site and surrounding area condition, as well as compatibility with the early earthwork stage. The framework begins with generating a variant of a gradient map to extract grids containing steep slopes. Nonlinear continuous large-scale slopes, such as hills and stockpiles, are then removed by utilizing the grid's Degrees of Freedom (DoF). The remaining grids are grouped using a region-growing algorithm to form a series of boundaries. To extract the target areas, road patches are generated by pairing boundaries and then calculating a series of centroids between those boundary pairs. Subsequently, patch connections are applied by comparing the cross-sectional properties of nearby patches. Finally, the connection results are refined by analyzing the distribution of grids. Thus, the method can be regarded as a hybrid of local feature analysis and graph theory.

The remainder of this paper is structured as follows: Section 2 provides a comprehensive review of previous work on road network extraction. Section 3 describes the proposed site extraction framework in detail. Section 4 presents a validation of the method using two ALS datasets. Finally, Section 5 discusses the conclusions and future work.

2 Literature Review

Transport network modeling is essential task for the subsequent tasks in many domains [13]. Over two decades ago, researchers began exploring the feasibility of using MLS and integrated sensors to capture 3D road models [14]. As-built models of transport infrastructure can be used for traffic analysis, simulation, and optimization, supporting efficient planning, renovation, and system improvement throughout its service life [15, 16]. The conventional Scan-to-BIM workflow consists of object recognition, segmentation, and reconstruction. These processes are responsible for classifying point clouds with semantic tags, segmenting points based on assigned labels, and reconstructing each recognized object for further processing [17-19]. Thus, accurate and effective pavement extraction is crucial for successful Scan-to-BIM, as it narrows the focus area, reduces complexity, and enhances accuracy. However, it should be noted that almost all existing methods are developed for finished road networks through MLS and their core criteria introduced are not suitable for road construction sites. In general, road extraction methods can be categorized into feature-based, learning-based, and graph-based methods.

2.1 Feature-based Road Extraction

Feature-based methods are widely used in road object recognition and information extraction. These methods can be further divided into region growing, feature extraction, feature fitting, and cross-section analysis. Typically, first three approaches are combined sequentially to extract areas of interest [15]. Zhang et al. [20] used region growing to extract the road surface, followed by intensity variance detection, B-spline and Alpha-shape techniques to create a pavement curve model. Such cooperation can also be found in Yadav et al. [21]. A two-step framework that first extracted local features in each grid and clustered smooth grids using a predefined threshold. Then, a plane fitting step was applied to refine the pavement extraction results. Rodríguez-Cuenca et al. [22] collaborated morphological image processing with grid-based local features analysis to precisely depict the road boundaries. Cross-section analysis methods normally create cross-sections along scanning trajectories or road markings [23, 24]. Pavement extraction is then performed by detecting road curbs or consecutive markings. Yang et al. [23] sliced the datasets along scanning lines and a moving window operator was applied to filter out irrelevant points as well as detecting curbs based on predefined patterns. Similarly, Guan et al. [25] developed algorithms to detect curbs using elevation and slope differences for automated road information extraction. Overall, feature-based methods are effective for identifying pavement boundaries by creating gradient maps, calculating elevation differences or detecting linear patterns, followed by numerical model fitting to generate detailed curve or surface models.

2.2 Learning-based Road Extraction

Like fused approaches in Scan-to-BIM, one or multiple procedures can be replaced by learning-based methods, such as curbs extraction and curve fitting [7, 26, 27]. Yang et al. [28] introduced a binary kernel descriptor (BKD) for encoding as-built point clouds, combined with a random forest classifier to extract curbs and road markings. Similarly, Soilán et al. [29] combined heuristic rules and unsupervised learning models to differentiate between pavement and sidewalks. To acquire better performance, Ma et al. [30] used satellite imagery and a deep learning framework, BoundaryNet, for improving road boundary extraction results. This hybrid method fed curb extraction results into a sequential refining model within BoundaryNet. Wei et al. [31] applied a reinforcement learning (RL) algorithm for curve fitting in complex 3D highway modeling. Road curbs are also commonly used in HD map generation tasks as indicators for pavement extraction [6].

2.3 Graph-based Road Extraction

Graph-based methods are less common as they require supplementary information such as transport network maps. Boyko et al. [32] developed a method using 2D road network maps to divide urban area point cloud into suitable size patches along optimized Cardinal splines. Then, identifying road networks through local elevation changes in patches. In contrast, Ma et al. [33] applied PointNet++ for initiating a rough road surface extraction and refined results using a two-step graph-based method.

3 Methodology

In this section, the proposed framework for extracting road network construction sites will be elaborated in detail. Compared with the subsequent parametric modeling in Scan-to-BIM for road construction, target area extraction is more challenging due to the complex site conditions and the ALS dataset utilized. This framework consists of four main steps: boundary grids candidate extraction, irrelevant grids removal, road patch generation and connection, and boundary grids refinement (Figure 1). The core idea lies in the road patch generation and connection, which utilizes cross-sectional properties to connect patches and form large network clusters. This step effectively extract the target area with different progress and layouts from its surroundings.

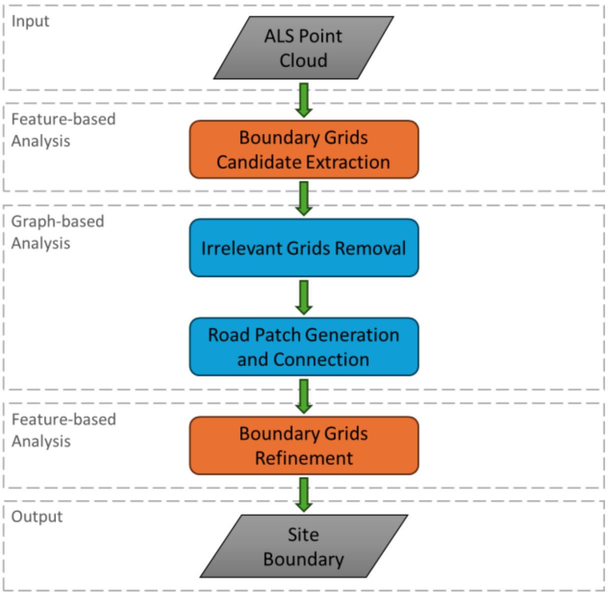

Figure 1. Workflow of the proposed road network construction site extraction framework.

3.1 Boundary Grids Candidate Extraction

Conventional methods for directly extracting ground surface points, such as those based on smoothness or edge detection, are not suitable for road networks under construction captured by ALS. Two main technical challenges identified are monotonous roughness and linear patterns across the entire field. In road construction sites, there is initially no significant roughness difference between the base course and its surrounding areas. Furthermore, unique wave-like patterns in ALS dataset complicates edge detection methods that rely on point distribution analysis. Its uniform distribution causes common local features, such as linearity, planarity, and omni-variance, to yield similar numerical values for areas with and without edges. As a result, instead of directly extracting the ground surface or applying edge detection, we opted to roughly extract boundary candidates using a gradient change ratio map (GCR).

The GCR map is a variant of the gradient map, designed to be more effective for large-scale areas. Initially, the x-y plane is divided into square-shaped grid cells with an empirical edge length of 1.5 m [34, 35]. The GCR is then calculated using the formula shown in Equation (1).

$$GCR = \frac{h_a - h_b}{D_{ab}} \tag{1}$$

where a and b represent the highest and lowest points within the same grid, respectively. Here, h_a and h_b are the elevations of the two points, and D_{ab} is the distance between the two points on the x-y plane. Equation (1) thus computes the gradient change ratio on the plane for each grid. Grids with GCR values exceeding $\mu + \alpha \cdot \sigma$ are defined as boundary candidates and prepared for irrelevant point removal. As an empirical parameter, the factor α is set to 1 for all cases.

3.2 Irrelevant Grids Removal

Irrelevant grid removal aims to eliminate grids belonging to hills and stockpiles that form large-scale nonlinear continuous slopes. This process uses the centroid of each grid as a node and creates a graph by connecting these nodes with edges. For a given group of candidate grids, if their width is more than twice the grid size, the grids in inner layer will have a DoF higher than 6, indicating that at least six grids are adjacent to them. To locate all irrelevant grids, those with a DoF of 7 or 8 are removed first. In the second step, grids with a reduced DoF after the initial removal are also eliminated to completely remove irrelevant areas. Following this, a region growing with an elevation criterion is applied to the remaining grids to cluster adjacent grids together. However, during this removal process, some grids containing boundaries of road construction sites may also be removed, as they are often adjacent to hills or trenches. These grids can still be retrieved through interpolation between the two ends or by fusing the grids with edge detection results. However, this retrieval process falls outside the scope of this paper.

3.3 Road Patch Generation and Connection

After removing irrelevant grids and the subsequent region-growing process, the adjacent grids are grouped into numerous clusters with either linear or random shapes. To precisely and automatically extract the boundaries of the construction site and establish connectivity between road segments under construction, road patch generation and connection are developed.

Road patch generation consists of two main steps: boundary pairing and centroid computation. In the boundary pairing step, a pair search is conducted within a given radius for each boundary, and all nearby boundaries with a certain proportion of grids within the range are stored. In the centroid computation step, the centroids of paired grids between two paired boundaries are calculated on the x-y plane. The patch is then generated based on the resulting centroids on two ends. The introduction of centroid computation serves two purposes: (1) to provide centroids for locating the two ends of the patches, and (2) to ensure that the patch is formed in a regular shape, even when the two paired boundaries have different lengths. For each grid, it should be noted that centroids are computed between the grid itself and its closest grid, as well as the neighbors of the closest grid in the paired boundary. This approach ensures a relatively smooth transition when curves are represented by staggered grids.

The key idea behind patch connection is similar to the region-growing algorithm. The seed and its neighboring properties are defined as the cross-sections at the ends of each patch. To handle complex road layouts, such as roundabouts, T-junctions, crossroads, and traffic islands, loose criteria are introduced to ensure flexibility. The cross-section is defined by three points: two paired grid centroids and their calculated centroid. The centroids of the two grids use the highest values on the z-axis within their respective grids as their elevation, while the calculated centroid's elevation is derived from the average lowest z-axis values of the two grids. By defining these three points for each cross-section, a triangular regular network (TRN) is established for each patch. This structure allows for easy analysis of the properties at the ends of patches. To evaluate connectivity, two criteria are applied: the aspect ratio (AR) and elevation. The aspect ratio is derived from the difference between the average elevation of two paired grids, $h_{A.max}$, and the elevation of the computed centroid, $h_{A.min}$, divided by the distance between the two centroids of the two paired grids, G_1 and $G_1{}'$ on the x-y plane as shown in Equation (2).

Proximity checking is a prerequisite for connectivity inspection. If the cross-section at one end of a patch is close to that of another, connectivity inspection is applied to determine their relationship. As shown in Equation (3), two road patches are grouped into the same cluster when both the AR and the elevation deviation are smaller than the respective tolerances, δ_{ar} and δ_e. The top ten largest clusters are then output and prepared for refinement.

$$AR = \frac{h_{A.max} - h_{A.min}}{\lVert G_1 - G_1{}' \rVert} \tag{2}$$

$$\frac{\lvert AR_i - AR_j \rvert}{min\left(AR_i, AR_j\right)} \leq \delta_{ar} \tag{3}$$

3.4 Boundary Clusters Refinement

Although road patch connections can form a series of large clusters and distinguish them from surrounding neighbors, the main components of some top-ranked clusters may still belong to fragments of irrelevant areas. To address this issue, cluster refinement is introduced to eliminate unwanted large clusters by analyzing the distribution of grid centroids at different resolutions (grid sizes). As the grid size increases, more centroids are included in each grid, resulting in a higher proportion of grids with nonlinear centroids inside. Two indicators, scale-invariant anisotropy and surface area, are used for refinement. Scale-invariant anisotropy ranges from 0 to 1 and increases with the level of randomness in the distribution, while surface area is calculated using a convex hull algorithm, where smaller surface areas indicate more linear distributions. By applying cross-inspection with these two criteria, irrelevant clusters can be effectively identified and removed.

4 Case Study

In this case study, a highway construction site in New South Wales, Australia was selected as the target. The selected area is approximately 1 km by 1 km, and the raw datasets were processed using commercial software to remove non-ground points. The site features complex layouts, including roundabouts, T-junctions, crossroads, and traffic islands. Additionally, due to weather conditions, irrelevant patterns such as truck ruts, mud, and ponding are visible in aerial images. Surrounding the site, temporary roads, hills, and a series of large-scale stockpiles further complicate the extraction of the construction site.

Two datasets were collected on 24 February 2023 and 18 March 2023 to monitor the earthwork at the construction site. As shown in Figure 2b, additional traffic lanes have been excavated on the top-left and bottom-right corners of the roundabout during the past 3.5 weeks. Furthermore, the newly added segments have varying widths, ranging from 8 meters to 15 meters. This information can be used as a reference for determining the search radius in boundary pairing. The ground truth (GT) was generated by manually segmenting the results of irrelevant grid removal, providing a clearer boundary for comparison.

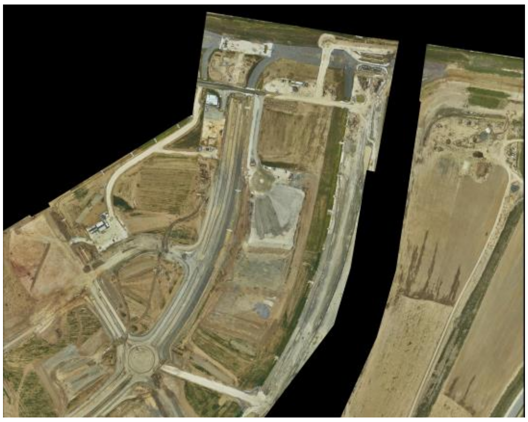

(a)

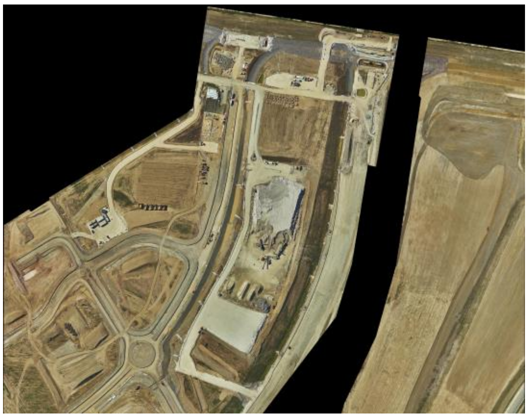

(b)

Figure 2. Aerial images of two datasets: (a) captured on 24 February 2023; (b) captured on 18 March 2023.

4.1 Boundary Grids Extraction

To extract boundary candidates, we applied the GCR to each grid to identify candidates with large elevation changes exceeding the sum of the average and standard deviation of GCR. As shown in Figure 3a, the resulting candidates contain hills and stockpiles located around the construction site. After applying irrelevant grid removal, the grids with nonlinear continuous slopes in these areas are removed. Only a few fragments remain in the datasets, as shown in Figure 3b. This process significantly reduces the number of grids introduced into subsequent road patch processing. Moreover, it prevents irrelevant grids from forming patches with other site boundaries, which could otherwise degrade the extraction results.

4.2 Road Patch Processing and Refinement

During the boundary pairing process, the search radius is set to 20 meters, which is slightly larger than the widest part of the entire road network. In this case, if one boundary has at least half of its grids located within this distance from another boundary, they are marked as paired boundaries. Road patch generation is then conducted based on these boundary pairs. Once the generation is completed, proximity and connectivity checks are initiated. The proximity radius threshold R is set to 10 meters, which is half the search radius used in the boundary pairing process. The tolerance for elevation (δ_e) and aspect ratio (δ_{ar}) are set to 10% and 30%, respectively. During the validation process, we observed that δ_{ar} values ranging from 30% to 50% produced similar results. However, due to the presence of T-junctions, where the width of certain areas changes dramatically, δ_{ar} cannot be set below 30%. Lower values lead to failure of grid extractions in those areas. In contrast, high δ_{ar} will include surrounding areas with dissimilar cross-sectional properties, which hinders the subsequent patch processing.

24 Feb 2023 18 Mar 2023

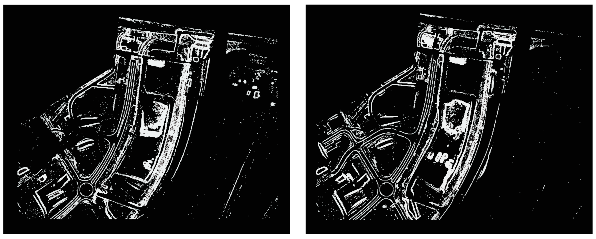

(a)

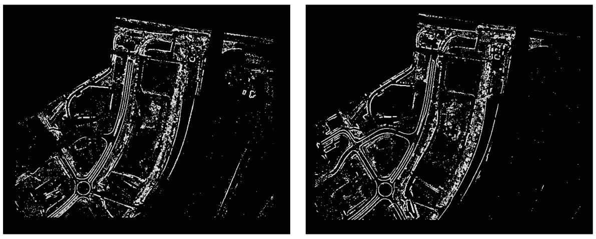

(b)

Figure 3. Results of boundary grids extraction: (a) Candidate grids on 24 February and 18 March 2023; (b) Irrelevant grid removal results on 24 February and 18 March 2023.

As shown in Figure 4a, several irrelevant red areas are extracted due to their large size. However, these clusters can be easily classified by inspecting the trends of local feature changes as the resolution decreases, given that the fragments and short boundaries are distributed randomly. During this process, the upper and lower bounds for the grid size are set at 7.5 meters and 4.5 meters, respectively. This ensures that the new grid contains at least three centroids of the old 1.5 meters grids without including multiple boundaries belonging to the roads. For each cluster, the number of grids with anisotropy and surface area exceeding the average values will increase due to the higher level of randomness introduced during the change of resolution. as the grid size approaches the upper bound, the proportion of grids with exceeded values in irrelevant clusters will first surpass 50%. By utilizing this principle, nearly all irrelevant red clusters are successfully removed, as shown in Figure 4b.

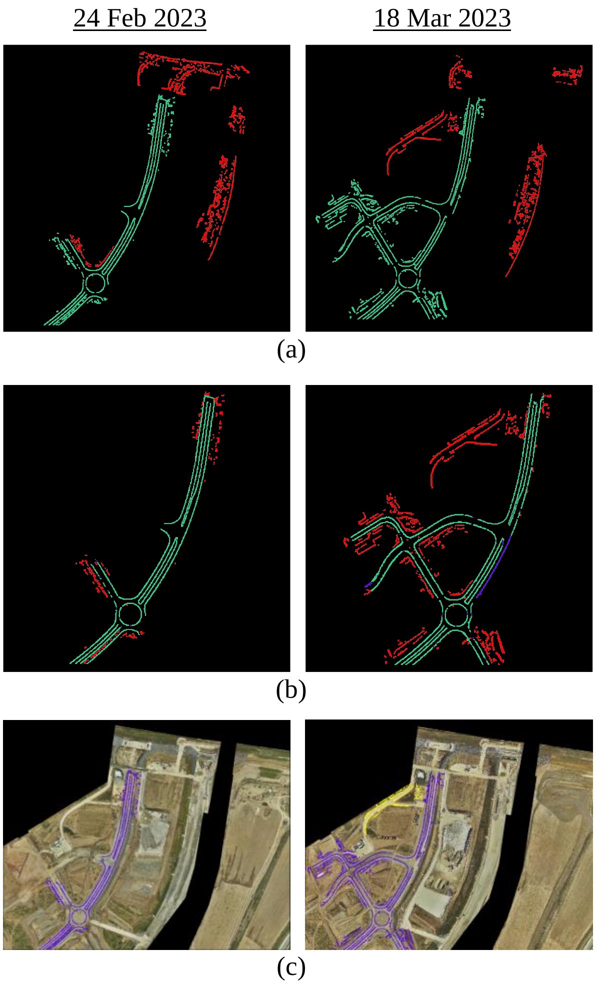

Figure 4. Results of road construction site boundary extraction: (a) Top 10 largest clusters on 24 Feb and 18 Mar 2023; (b) Correct boundaries (green) with missing parts (blue) and excess parts (red) on 24 Feb and 18 Mar 2023; and (c) Overlaid site boundaries on aerial images on 24 Feb and 18 Mar 2023.

The performance evaluation was conducted by calculating the overlap ratio of grids between the extraction results and the GT. As shown in Table 1, the accuracy of the proposed framework for the two datasets is 99.59% and 94.50%, respectively. The deviation is mainly caused by the rearrangement of stockpiles adjacent to the missing boundary, highlighted in blue in Figure 4b on 18 March. This rearrangement results in more fragments of stockpiles remaining near the missing boundary, which affects patch generation and connection. Additionally, the excess ratio for the second dataset is significantly higher than that of the first, at approximately 58.32%. This is clearly visible in Figure 4b on 18 March, where a curved temporary road is highlighted in red. Over the past 3.5 weeks, a series of road barriers have been installed along this temporary road, providing distinctive geometric features that help generate a more complete road boundary. Due to its clear linear pattern, the temporary road was retained during refinement. In Figure 4c, the extracted site boundaries are overlaid on aerial images. The grids align precisely along the boundaries of the road network construction site and can be updated to reflect changes in the construction process. This demonstrates that the proposed method can reliably provide the target area for the subsequent Scan-to-BIM process.

Table 1. Results of road construction site extraction with accuracy (%) and excess ratio (%).

Number of Grids	*24-Feb*	*18-Mar*
Site Boundary	2,466	5,008
Ground Truth	1,944	2,781
Overlapped	1,936	2,628
Accuracy (%)	99.59	94.50
Excess	530	2,380
Excess Ratio (%)	27.26	85.58

5 Conclusions

This paper presented an automated site extraction framework to support Scan-to-BIM progress monitoring in road construction. By leveraging the advantages of local feature analysis and graph theory, this hybrid approach successfully segments the target area from its surroundings. The application of GCR candidate extraction reduces computational requirements and addresses the challenges posed by complex site conditions, which conventional pavement extraction methods struggle to handle. The irrelevant grids removal process effectively fragments grids of nonlinear slopes into small clusters, which can then be easily eliminated. Patch generation and connection provide a feasible solution for segmenting the construction site from the surrounding area with similar cross-sectional features. The criteria utilized are well-suited for handling complex road shapes and layouts. After cluster refinement, the framework achieves a minimum accuracy of 94.50%. The results indicate that the proposed method can be applied to datasets with different road layouts and construction progress, highlighting its generality and potential for datasets from other projects.

Some limitations remain in the proposed framework.

The centroid generation process lacks stability when curves cause multiple grids to select the same closest grid in the paired boundary during centroids computation. Moreover, to ensure a clear end edge when paired boundaries have different lengths, we apply a threshold to handle this case. However, both strategies may result in the omission of centroids in certain specific positions. Thus, for future work, two modifications and a missing parts retrieve step can be incorporated into the framework to further improve its performance. These modifications aim to enhance the accuracy of boundary pairing and centroid computation during road patch generation, as these steps significantly impact overall accuracy. Boundary searching could introduce more multiple paring criteria, rather than relying solely on distance. Centroid calculation could also be refined by incorporating predefined shapes to enhance the smoothness and continuity of centroid transitions. The missing grids retrieve process could be achieved by overlapping boundary curves derived from elevation scalar fields onto the extraction results. Since the target areas have already been identified, the focus would shift to curves that connect extracted grids located far apart. By inspecting grids along these focused curves, missing grids could be effectively retrieved.

Acknowledgement

This research was supported by funding from the Australian Research Council (ARC) under Grant number IH210100048 ARC Research Hub for Resilient and Intelligent Infrastructure Systems (RIIS). We would also like to express our gratitude to GeoAI for their support and collaboration.

References

[1] Y. Chong Heap, R. Lopez, J. Wang, X. Wang, and Z. Zhao, *Comparative Analysis on the Adoption and Use of BIM in Road Infrastructure Projects.* Journal of Management in Engineering, 2016. **32**(6): p. 05016021.

[2] A. Costin, A. Adibfar, H. Hu, and S.S. Chen, *Building Information Modeling (BIM) for transportation infrastructure – Literature review, applications, challenges, and recommendations.* Automation in Construction, 2018. **94**: p. 257-281.

[3] T. Patel, B.H.W. Guo, and Y. Zou, *A scientometric review of construction progress monitoring studies.* Engineering, Construction and Architectural Management, 2021. **ahead-of-print**(ahead-of-print).

[4] Z. Jiang, X. Shen, M. Ibrahimkhil, K. Barati, and J. Linke. *Scan-VS-BIM for real-time progress monitoring of bridge construction project*. in *ISPRS Annals of the Photogrammetry, Remote Sensing and Spatial Information Sciences*. 2022.

[5] M.H. Ibrahimkhil, X. Shen, K. Barati, and C.C. Wang *Dynamic Progress Monitoring of Masonry Construction through Mobile SLAM Mapping and As-Built Modeling*. Buildings, 2023. **13**, DOI: 10.3390/buildings13040930.

[6] C. Ye, H. Zhao, L. Ma, H. Jiang, H. Li, R. Wang, M.A. Chapman, J.M. Junior, and J. Li, *Robust Lane Extraction From MLS Point Clouds Towards HD Maps Especially in Curve Road.* IEEE Transactions on Intelligent Transportation Systems, 2022. **23**(2): p. 1505-1518.

[7] B. Suleymanoglu, M. Soycan, and C. Toth *3D Road Boundary Extraction Based on Machine Learning Strategy Using LiDAR and Image-Derived MMS Point Clouds*. Sensors, 2024. **24**, DOI: 10.3390/s24020503.

[8] K. Karila, L. Matikainen, E. Puttonen, and J. Hyyppä, *Feasibility of Multispectral Airborne Laser Scanning Data for Road Mapping.* IEEE Geoscience and Remote Sensing Letters, 2017. **14**(3): p. 294-298.

[9] E. Che, J. Jung, and M.J. Olsen, *Object Recognition, Segmentation, and Classification of Mobile Laser Scanning Point Clouds: A State of the Art Review.* Sensors, 2019. **19**(4).

[10] K. Mirzaei, M. Arashpour, E. Asadi, H. Masoumi, Y. Bai, and A. Behnood, *3D point cloud data processing with machine learning for construction and infrastructure applications: A comprehensive review.* Advanced Engineering Informatics, 2022. **51**: p. 101501.

[11] Y. Xu, X. Shen, S. Lim, and X. Li, *Three-Dimensional Object Detection with Deep Neural Networks for Automatic As-Built Reconstruction.* Journal of Construction Engineering and Management, 2021. **147**(9): p. 04021098.

[12] Y. Guo, X. Shen, J. Linke, Z. Wang, and K. Barati *Quantification of Structural Defects Using Pixel Level Spatial Information from Photogrammetry*. Sensors, 2023. **23**, DOI: 10.3390/s23135878.

[13] R. Wang, J. Peethambaran, and D. Chen, *LiDAR Point Clouds to 3-D Urban Models$:$ A Review.* IEEE Journal of Selected Topics in Applied Earth Observations and Remote Sensing, 2018. **11**(2): p. 606-627.

[14] I. Kiichiro, T. Jun-ichi, A. Yoshiharu, and H. Takumi. *A Mobile Mapping System for road data capture based on 3D road model*. in *2006 IEEE Conference on Computer Aided Control System Design, 2006 IEEE International Conference on Control Applications, 2006 IEEE International Symposium on Intelligent Control*. 2006.

[15] M. Soilán, A. Sánchez-Rodríguez, P. del Río-Barral,

C. Perez-Collazo, P. Arias, and B. Riveiro *Review of Laser Scanning Technologies and Their Applications for Road and Railway Infrastructure Monitoring*. Infrastructures, 2019. **4**, DOI: 10.3390/infrastructures4040058.

[16] P. Wei, L. Yan, H. Xie, and M. Huang, *Automatic coarse registration of point clouds using plane contour shape descriptor and topological graph voting.* Automation in Construction, 2022. **134**: p. 104055.

[17] N. Abreu, A. Pinto, A. Matos, and M. Pires *Procedural Point Cloud Modelling in Scan-to-BIM and Scan-vs-BIM Applications: A Review*. ISPRS International Journal of Geo-Information, 2023. **12**, DOI: 10.3390/ijgi12070260.

[18] D. Rebolj, Z. Pučko, N.Č. Babič, M. Bizjak, and D. Mongus, *Point cloud quality requirements for Scan-vs-BIM based automated construction progress monitoring.* Automation in Construction, 2017. **84**: p. 323-334.

[19] Q. Wang, J. Guo, and M.-K. Kim *An Application Oriented Scan-to-BIM Framework*. Remote Sensing, 2019. **11**, DOI: 10.3390/rs11030365.

[20] Z. Zhang, J. Li, Y. Guo, C. Yang, and C. Wang, *3D Highway Curve Reconstruction From Mobile Laser Scanning Point Clouds.* IEEE Transactions on Intelligent Transportation Systems, 2020. **21**(11): p. 4762-4772.

[21] M. Yadav and A.K. Singh, *Rural Road Surface Extraction Using Mobile LiDAR Point Cloud Data.* Journal of the Indian Society of Remote Sensing, 2018. **46**(4): p. 531-538.

[22] B. Rodríguez-Cuenca, S. García-Cortés, C. Ordóñez, and M.C. Alonso, *An approach to detect and delineate street curbs from MLS 3D point cloud data.* Automation in Construction, 2015. **51**: p. 103-112.

[23] B. Yang, L. Fang, and J. Li, *Semi-automated extraction and delineation of 3D roads of street scene from mobile laser scanning point clouds.* ISPRS Journal of Photogrammetry and Remote Sensing, 2013. **79**: p. 80-93.

[24] L. Ma, Y. Li, J. Li, C. Wang, R. Wang, and M.A. Chapman *Mobile Laser Scanned Point-Clouds for Road Object Detection and Extraction: A Review*. Remote Sensing, 2018. **10**, DOI: 10.3390/rs10101531.

[25] H. Guan, J. Li, Y. Yu, M. Chapman, and C. Wang, *Automated Road Information Extraction From Mobile Laser Scanning Data.* IEEE Transactions on Intelligent Transportation Systems, 2015. **16**(1): p. 194-205.

[26] N. Wang, Z. Shi, and Z.J.C.J.o.R.S. Zhang, *Road boundary, curb and surface extraction from 3D mobile LiDAR point clouds in urban environment.* 2022. **48**(4): p. 504-519.

[27] J. Balado, J. Martínez-Sánchez, P. Arias, and A. Novo *Road Environment Semantic Segmentation with Deep Learning from MLS Point Cloud Data*. Sensors, 2019. **19**, DOI: 10.3390/s19163466.

[28] B. Yang, Y. Liu, Z. Dong, F. Liang, B. Li, and X. Peng, *3D local feature BKD to extract road information from mobile laser scanning point clouds.* ISPRS Journal of Photogrammetry and Remote Sensing, 2017. **130**: p. 329-343.

[29] M. Soilán, L. Truong-Hong, B. Riveiro, and D. Laefer, *Automatic extraction of road features in urban environments using dense ALS data.* International Journal of Applied Earth Observation and Geoinformation, 2018. **64**: p. 226-236.

[30] L. Ma, Y. Li, J. Li, J.M. Junior, W.N. Gonçalves, and M.A. Chapman, *BoundaryNet: Extraction and Completion of Road Boundaries With Deep Learning Using Mobile Laser Scanning Point Clouds and Satellite Imagery.* IEEE Transactions on Intelligent Transportation Systems, 2022. **23**(6): p. 5638-5654.

[31] Y. Wei, Z. Zhang, X. Huang, Y. Lin, and W. Liu, *3D HIGHWAY CURVE RECONSTRUCTION FROM MOBILE LASER SCANNING POINT CLOUDS THROUGH DEEP REINFORCEMENT LEARNING.* Int. Arch. Photogramm. Remote Sens. Spatial Inf. Sci., 2023. **XLVIII-1/W2-2023**: p. 55-61.

[32] A. Boyko and T. Funkhouser, *Extracting roads from dense point clouds in large scale urban environment.* ISPRS Journal of Photogrammetry and Remote Sensing, 2011. **66**(6, Supplement): p. S2-S12.

[33] H. Ma, H. Ma, L. Zhang, K. Liu, and W. Luo *Extracting Urban Road Footprints from Airborne LiDAR Point Clouds with PointNet++ and Two-Step Post-Processing*. Remote Sensing, 2022. **14**, DOI: 10.3390/rs14030789.

[34] B. Yang, R. Huang, Z. Dong, Y. Zang, and J. Li, *Two-step adaptive extraction method for ground points and breaklines from lidar point clouds.* ISPRS Journal of Photogrammetry and Remote Sensing, 2016. **119**: p. 373-389.

[35] Y. Zhou, R. Huang, T. Jiang, Z. Dong, and B. Yang, *Highway alignments extraction and 3D modeling from airborne laser scanning point clouds.* International Journal of Applied Earth Observation and Geoinformation, 2021. **102**: p. 102429.